Strahlenther Onkol 2012 · 188:346–352
DOI 10.1007/s00066-011-0066-z
Received: 23 October 2010
Accepted: 12 December 2011
Published online: 9 March 2012

S.K. Hui[1] · E. Lusczek[1] · T. DeFor[2] · K. Dusenbery[1] · S. Levitt[1,3]
[1] Department of Therapeutic Radiology – Radiation Oncology, University of Minnesota Medical School, Minneapolis
[2] Biostatistics and Informatics Core, Masonic Cancer Center, University of Minnesota Medical School, Minneapolis
[3] Dept of Onkol-Patol, Karolinska Institutet, Stockholm

Three-dimensional patient setup errors at different treatment sites measured by the Tomotherapy megavoltage CT

Recent developments in radiation therapy have focused on highly conformal radiation that can target a tumor, while avoiding critical organs to reduce radiation toxicity [1, 2]. Benefits have been reported for head and neck (H&N) and prostate cancers [3, 4, 5, 6, 7]. In the last decade, image-guided radiation therapies (IGRT) have allowed precise conformal radiation therapy for different diseases [8, 9, 10, 11, 12, 13, 14, 15, 16, 17, 18, 19]. With such targeted treatments, precision in delivery of the radiation is more critical than ever [20, 21, 22, 23].

The Tomotherapy unit is an IGRT machine that delivers radiation helically and an onboard megavoltage CT (MVCT) detector supports image guidance [24, 25, 26, 27, 28, 29]. The conformal radiation treatment delivered by the Tomotherapy unit has the potential to enhance the therapeutic ratio (dose to tumor/organs at risk (OARs)). This is achieved by reducing the radiation dose delivered to healthy tissues and OARs [30]. Due to variations in patient positioning and variation in organ shape and volume, the delivered radiation dose may differ from the highly conformal planned dose [26, 29, 31, 32, 33, 34, 35]. In this study, our goal was to measure and compare setup error at different treatment sites and setup variation with time treated with Tomotherapy.

Methods and materials

Using MVCT scans, we reviewed the day-to-day variations in patient positioning during Tomotherapy treatment. Details of MVCT detector characteristics used in the Tomotherapy machine are published elsewhere [28]. In brief, a radiation source with an average energy of 1.36 MeV and xenon gas detector array operated at 5 mm atm pressure are used to generate a MVCT image with a field of view of 40 cm. MVCT acquisition modes of fine, normal, and course can be used to scan an object with slice thicknesses of 2, 4, and 6 mm, respectively.

MVCT scans were performed before each treatment fraction for all patients treated using the Tomotherapy machine. An aquaplast mask was used for H&N immobilization and VacLok (Med-Tec Inc., Orange City, IA, USA) was used for all other extra cranial immobilization (chest, abdomen, legs, prostate, total marrow irradiation (TMI), etc.). This retrospective study was approved by the University of Minnesota Institutional Review Board. We analyzed the pretreatment megavoltage CT images for 259 patients treated from 2005–2008. In total 6,465 MVCT scans were done for patient localization with site-specific scans taken of the pelvis (n = 949), chest (735), H&N (1,567), legs (218), prostate (2,711), spine (143), and TMI (42). The H&N category includes all head and neck cancers, including brain tumors and nasopharyngeal tumors. The chest category includes lung, sternum, mediastinum, mantle, and esophageal tumors. The pelvis category includes cancer treatment of the pelvis, cervix, and uterus. Prostate cancers, which account for one-third of the data, were placed in a unique category. The legs category includes all cancers of the tissues and bone in the legs. Due to unique challenges in patient localization, the TMI data were placed in a unique category.

Pretreatment MVCT and planning kVCT images were fused using the "bone and soft tissue" fusion registration mode on the Tomotherapy user interface. Fusion between MVCT scan and kVCT images were based on rigid body registration in three translational and one rotational degree of freedom as previously reported by Sara et al. [36]. Bony anatomy and other anatomical structures near the tumor location were matched and verified by the staff physician. The displacement coordinates required to match MVCT with pretreatment (baseline) kVCT images provide setup error along the translational directions (x, y, and z) for each sites. The three-dimensional (3D) average displacement is then calculated from individual displacement in x, y, and z directions using

$$\sqrt{x^2+y^2+z^2}$$

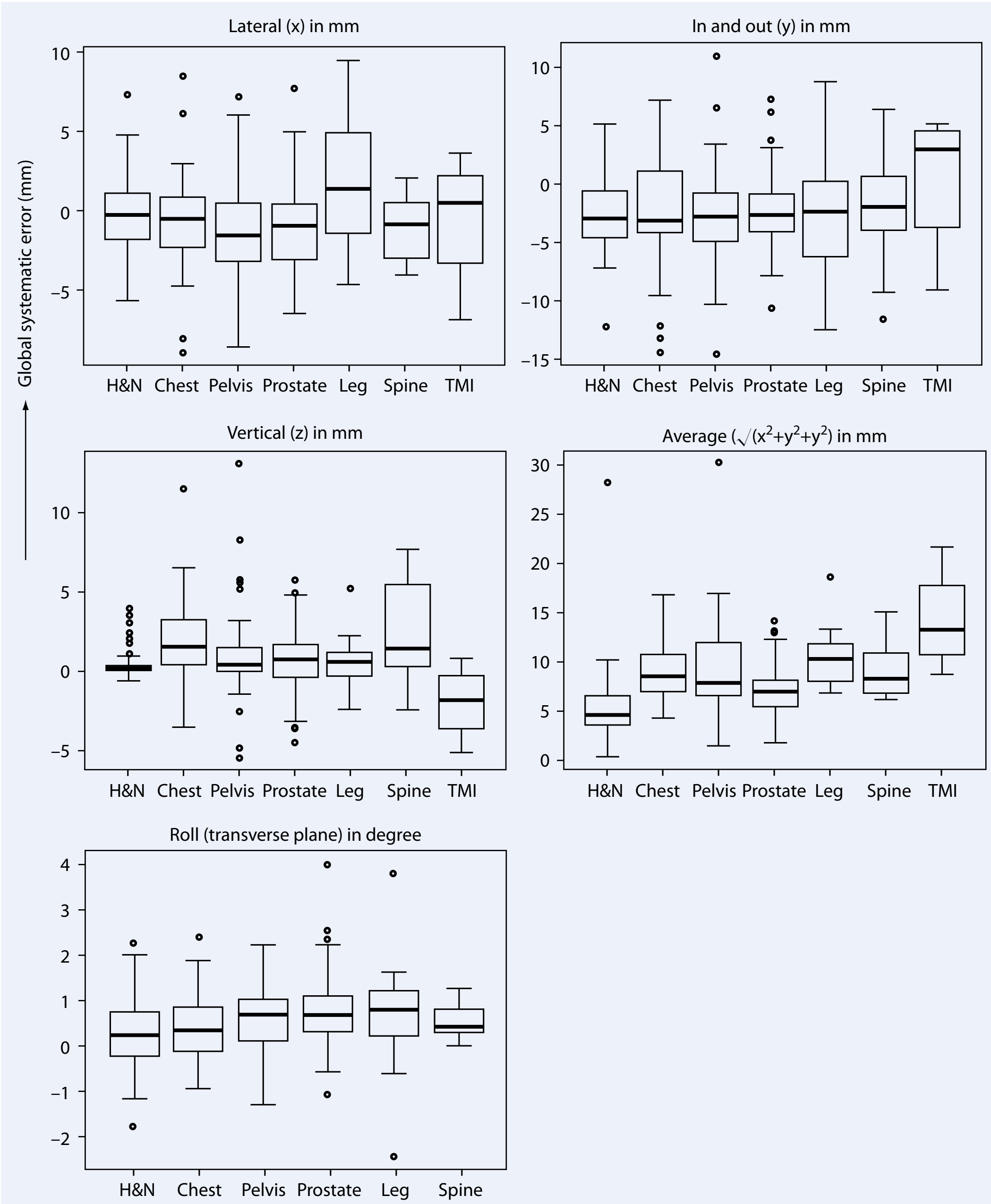

Fig. 1 ◀ Global systematic error is presented by box plot for all treatment regions. *Top* Systematic error in x (*left*) and y (*right*), *middle* systematic error in z (*left*) and 3D average of x, y, and z (*right*), *bottom* systematic error in the rotational direction. Rotation was not measured in total marrow irradiation (*TMI*) patients. *H&N* head and neck

Patient-specific systematic error is defined as the mean of 3D setup error for a patient for multiple treatment fractions and random error can be defined as the standard deviation. Global systematic error is defined as the mean of the systematic error distribution of the population treated at the specific site and standard deviation of the global systematic error is calculated from patient-to-patient variation in systematic errors.

For TMI treatments, patients were initially aligned using laser beams at the virtual isocenter matched with tattoos located on the head, chest, and abdomen, and MVCT image scans were performed in the H&N, chest, and abdominal regions to cover all critical organs [37, 38]. Image fusion registration coordinates of the H&N MVCT scans were used for initial patient localization. Following this, chest MVCT scans were used to align the patient. Finally, abdominal MVCT scans were used to align the lower portion of the patient. Rotational coordinates were not used during fusion registration to avoid the complication of averaging rotational uncertainty.

Statistical methods

For each treatment fraction, the patient's displacement in lateral (x), in and out of the tomotherapy gantry (y), and vertical (z) directions were recorded. Global systematic and random errors were calculated as previously explained. Box plots were employed to show the distribution of global systematic error in the x, y, z and R direction in a graphical manner [39]. The lower end of the box delineates the 25^{th} percentile of the data. The upper end of the box delineates the 75^{th} percentile of the data. The mid/dark line is the median. The whiskers extend to a maximum of 1.5 times the interquartile range. The points outside the whiskers are considered outliers.

Statistical comparisons of the absolute displacement across site and time (i.e., number of fractions) were performed by using a general linear mixed model. This analysis takes into account the repeated measures within patients and the correlation that exists between these repeated measures versus the correlation across patients which are more independent of each other [40]. Among the models in which a difference was detected, the Tukey–Kramer method identified which pair-wise comparisons resulted in statistically significant differences [41]. A p value ≤ 0.05 was considered significant. All analyses were performed using SAS V9 software (SAS Institute, Cary, NC, USA).

Results

Global systematic error for all treatments sites are presented in the box plots in **Fig. 1**. For each individual treatment region, the median systematic error was highest in the y direction and lowest in the z direction, except for the chest category where displacement in x was greater than displacement in z. Details of global systematic and random variations in the x, y, and z direction for individual treatment sites are tabulated (**Tab. 1**). The global systematic errors were measured to be less than 3 mm in each direction with increasing order of errors for different sites: H&N, prostate, chest, pelvis, spine, legs, and TMI. Random component of all the sites were higher ranging from 2–6.33 mm except for TMI.

The differences in displacements between treatment sites in the lateral (x), craniocaudal (y), and vertical (z) direction were significant ($p < 0.01$) as shown in **Tab. 2**. Rotational set-up error was not significant. In the lateral direction (x), the average displacements for the H&N category were significantly less than for chest, abdomen, prostate, and leg categories. Average displacements in the prostate were significantly less than for leg sites. Average displacements in the chest, abdomen, prostate, and leg were not significantly

Abstract · Zusammenfassung

Strahlenther Onkol 2012 · 188:346–352 DOI 10.1007/s00066-011-0066-z

S.K. Hui · E. Lusczek · T. DeFor · K. Dusenbery · S. Levitt

Three-dimensional patient setup errors at different treatment sites measured by the Tomotherapy megavoltage CT

Abstract

Background and purpose. Reduction of interfraction setup uncertainty is vital for assuring the accuracy of conformal radiotherapy. We report a systematic study of setup error to assess patients' three-dimensional (3D) localization at various treatment sites.

Patients and methods. Tomotherapy megavoltage CT (MVCT) images were scanned daily in 259 patients from 2005–2008. We analyzed 6,465 MVCT images to measure setup error for head and neck (H&N), chest/thorax, abdomen, prostate, legs, and total marrow irradiation (TMI). Statistical comparisons of the absolute displacements across sites and time were performed in rotation (R), lateral (x), craniocaudal (y), and vertical (z) directions.

Results. The global systematic errors were measured to be less than 3 mm in each direction with increasing order of errors for different sites: H&N, prostate, chest, pelvis, spine, legs, and TMI. The differences in displacements in the x, y, and z directions, and 3D average displacement between treatment sites were significant ($p < 0.01$). Overall improvement in patient localization with time (after 3–4 treatment fractions) was observed. Large displacement (> 5 mm) was observed in the 75th percentile of the patient groups for chest, pelvis, legs, and spine in the x and y direction in the second week of the treatment.

Conclusion. MVCT imaging is essential for determining 3D setup error and to reduce uncertainty in localization at all anatomical locations. Setup error evaluation should be performed daily for all treatment regions, preferably for all treatment fractions.

Keywords

Setup error · MVCT imaging · Tomotherapy · Patient localization · Radiotherapy

Dreidimensionale Patienten-Setup-Fehler an unterschiedlichen Bestrahlungslokalisationen gemessen mittels Tomotherapie-Megavolt-CT

Zusammenfassung

Hintergrund und Ziel. Die Reduktion der interfraktionellen Setup-Ungenauigkeit ist von entscheidender Bedeutung, um die Genauigkeit der konformalen Strahlentherapie sicherzustellen. Wir berichten über eine systematische Untersuchung des Setup-Fehlers zur Bewertung der dreidimensionalen (3-D) Lagerungsgenauigkeit von Patienten mit unterschiedlichen Bestrahlungsregionen.

Patienten und Methoden. Von 2005–2008 wurden täglich Tomotherapie-Megavolt-CT-(MVCT-)Bilder von 259 Patienten aufgenommen. Wir analysierten 6465 MVCT-Bilder, um Setup-Fehler bei der Bestrahlung von Kopf und Hals, Thorax, Abdomen, Prostata, Beinen und des gesamten Knochenmarks (TMI) zu messen. Statistikvergleiche der absoluten Verschiebungen hinsichtlich der Bestrahlungsregion und der Zeit wurden in Rotation (R), seitlicher (x), kraniokaudaler (y) und vertikaler (z) Richtung vorgenommen.

Ergebnisse. Als globale systematische Fehler wurden in jeder Richtung Abweichungen von weniger als 3 mm in zunehmendem Maß bei den unterschiedlichen Bestrahlungsregionen gemessen: Kopf und Hals (H&N), Prostata, Brust, Becken, Wirbelsäule, Beine und gesamtes Knochenmark (TMI). Die Unterschiede der Abweichungen in x-, y- und z-Richtung und die durchschnittliche 3-D-Verschiebung waren bei den unterschiedlichen Bestrahlungsregionen signifikant ($p < 0{,}01$). Insgesamt wurde eine Verbesserung der Lagerungsgenauigkeit der Patienten im zeitlichen Verlauf (nach 3–4 Bestrahlungsfraktionen) beobachtet. Große Abweichungen (> 5 mm) in x- und y-Richtung wurden in der 75. Perzentile der Patientengruppe in der 2. Behandlungswoche bei Brust, Becken, Beinen und Wirbelsäule beobachtet.

Schlussfolgerung. MVCT-Imaging ist wichtig, um 3-D-Setup-Fehler festzustellen und Ungenauigkeiten der Lokalisierung in allen anatomischen Regionen zu reduzieren. Eine Setup-Fehlerermittlung sollte täglich für alle Bestrahlungsregionen und möglichst für alle Bestrahlungsfraktionen vorgenommen werden.

Schlüsselwörter

Setup-Fehler · MVCT-Imaging · Tomotherapie · Patientenlagerung · Strahlentherapie

Tab. 1 Global systematic error of x, y, z, 3D average, and R dimension

	Lateral (x) (mm)	Longitudinal (y) (mm)	Vertical (z) (mm)	Average $\sqrt{(x^2+y^2+z^2)}$	Roll (°)
Global systematic error					
Site					
H&N	−0.36	−2.59	0.42	5.11	0.26
Chest	−0.40	−2.15	1.81	8.58	0.45
Pelvis	−1.27	−2.70	0.72	9.05	0.81
Prostate	−1.32	−2.55	0.62	7.51	0.84
Legs	0.60	−1.79	0.82	9.97	0.42
Spine	−1.34	−2.11	1.51	9.03	0.53
TMI	−0.52	1.12	−1.73	15.73	
Variation in systematic error					
Site					
H&N	2.17	2.68	1.53	2.62	0.81
Chest	3.12	3.78	1.99	2.51	0.72
Pelvis	2.75	3.17	1.86	3.97	0.76
Prostate	2.54	2.74	1.59	2.87	0.77
Legs	4.45	4.19	2.10	2.47	1.32
Spine	2.01	5.21	2.93	2.69	0.45
TMI	4.41	4.76	1.67	4.87	
Magnitude of random error					
Site					
H&N	2.01	3.11	2.50	6.81	0.93
Chest	3.99	5.51	4.71	10.47	1.13
Pelvis	4.13	3.75	4.31	12.44	1.00
Prostate	3.76	3.03	3.91	10.55	0.72
Legs	4.79	5.45	5.70	11.33	1.01
Spine	5.07	3.41	4.44	11.96	1.02

H&N head and neck, **TMI** total marrow irradiation.

different from each other. In the cranio-caudal (y), direction the H&N average displacements were significantly less than those for chest and abdomen, but were not significant compared to prostate and leg. Average displacements of the prostate were significantly less than in chest and leg sites. In the vertical direction (z), average displacements for H&N were significantly less than for chest, abdomen, prostate, and leg. Overall, the average H&N displacement was significantly less than for any other site, and prostate displacement was significantly less than chest, abdomen, and leg. Rotation did not significantly differ between any two groups.

Variations in displacement for each treatment site on different days are shown in **Fig. 2**. Initial displacements in the z direction were higher in the first 3 days for almost all sites. This interfraction error improved after 3 days and remained stable afterwards. There was a significant improvement in the reduction of set-up error in the z direction over time ($p<0.01$), with a reduction in error of 0.3 mm per measurement episode. Overall displacements in the x ($p=0.34$) and y ($p\neq0.43$) directions did not improve over time.

Discussion

There were large differences in patient set-up uncertainty among treatment sites as shown in **Fig. 1** and **Tab. 1**. The variation in daily patient localization comes from subtle changes in three-dimensional patient localization within the Tomotherapy unit, as well as from volumetric and/or shape changes in the organ containing tumor and organs-at-risk. Reduced uncertainty in the H&N region is possibly due to use of a head mask. Large set up errors were observed in all TMI patients. In TMI treatments, patient localization is complicated due to a combination of factors, e.g., large field area, adjustment from multiple imaging of multiple areas, and the use of coarse imaging modalities for extra-cranial localization [42, 43]. Clearly, TMI patient localization will require further development to reduce uncertainty.

Overall setup error was highest in the z direction and lowest in the x direction. Variation in image scan mode can influence changes in y displacement. The majority of our patients were scanned in the normal mode of MVCT imaging. Our data demonstrate greater variation in the vertical (z) direction as has been reported for brain, H&N, prostate, and lungs [44]. In our study, we included the additional treatment areas of legs, pelvis, and TMI. We did not find any differences in set-up error between the two centers for H&N, prostate, or chest.

To investigate statistical differences in interfraction displacement between any two treatment regions, pair-wise comparisons were made. Among treatment regions, H&N differed significantly in all three directions and had the smallest overall localization uncertainty of any group. Prostate localization showed the next smallest displacement overall. Rotation did not significantly differ between any two groups.

Previous studies of interfraction treatment focused mostly on evaluating set-up error in individual treatment groups. Our large imaging database allowed us to perform a comparative study among various treatment sites and alignments with statistical significance. A comparative knowledge of setup variations at different sites will help develop strategies to reduce motion at different sites. It will provide

- identification of sites/regions that require more attention to reduce motion to achieve comparable dose delivery as with those sites with better localization and
- guidance to develop new treatments such as total marrow irradiation where the entire skeleton is being treated with highly targeted radiation [37, 38, 43].

Improvement in patient localization with time (after 3–4 treatment fractions) is an interesting phenomenon. We applied correction every day starting from the first treatment fractions and continued the same strategy for the entire treatment pe-

Tab. 2 Mixed procedure taking repeated measurements of x, y, z, and rotation (*R*) dimension within patient into account

		Mean (standard error) in x, y, z, R, and average									
	Patients (n)	x^a	p value	y^b		z^c		$\sqrt{(x^2+y^2+z^2)}^d$		R^e	
Site			< 0.01		< 0.01		< 0.01		< 0.01		0.20
H&N	60	2.2 (0.2)		3.5 (0.2)		2.0 (0.2)		5.3 (0.3)		0.8 (0.1)	
Chest	33	3.9 (0.3)		5.9 (0.3)		4.4 (0.3)		10.0 (0.4)		0.9 (0.1)	
Pelvis	44	4.2 (0.3)		5.7 (0.3)		3.3 (0.2)		9.1 (0.3)		1.0 (0.1)	
Prostate	99	3.5 (0.2)		4.0 (0.2)		3.5 (0.1)		7.4 (0.2)		0.9 (0.1)	
Leg	10	5.5 (0.6)		5.8 (0.6)		4.0 (0.5)		10.6 (0.7)		1.3 (0.2)	
Spine	10	4.3 (0.6)		4.5 (0.6)		4.1 (0.5)		9.0 (0.7)		0.9 (0.2)	
Time		−0.009	0.71	−0.03	0.30	−0.27	< 0.01	−0.23	< 0.01	−0.27	0.21

[a]**x**: H&N is different from all others; prostate is different from pelvis and leg[b]**y**: H&N is different from chest, pelvis, and leg; prostate is different from pelvis and leg[c]**z**: H&N is different from all others; chest is different from pelvis and prostate[d]**Average** $\sqrt{(x^2+y^2+z^2)}$: H&N is different from all others; chest is different from pelvis; prostate is different from pelvis and leg[e]**R**: H&N is different from leg; leg is different from spine.

riod. Significant improvements in the z direction after 4–5 fractions (first week) are observed for almost all treatment sites. This interesting phenomenon did not translate to the two other coordinates. Various other patterns of displacement were observed in x and y directions. In the lateral (x) direction, daily setup error was stable over days in H&N, abdomen, and prostate. On the other hand, the thoracic area and legs showed large variations in setup error on different days without any patterns. In the y direction, all treatment regions except legs had stable patterns of displacement.

Broggy et al. [45] recently showed reduced systematic error for prostate treatment for various correction strategies. Correction applied only during first fraction may not be sufficient for overall treatment [46]. For short treatment schedules (hypofractionation), correction during each fraction may also be important. Globally, there is no further improvement observed after the first week. It has been suggested that 3D imaging scans be used over the first few days [44]. Should this be the guiding rule for clinical practice, i.e., to use 3D images for patient localization only during the first week? We are concerned about this approach when individual accuracy becomes important. A time course analysis of displacements (**Fig. 2**) shows that there are large displacements (> 5 mm) in the 75th percentile of patients in the chest, pelvis, legs, and spine groups in the x and y directions, even for all treatment fraction in the second week of treatment. This may have important consequences for individual treatment delivery. It could be dangerous to couple target margin reduction techniques such as those seen in image-guided conformal radiotherapy (based on our knowledge of setup error in the population), if image-guided alignment is not used past the first week. The risk of relapse from underdosing may be high compared to benefit of reduced toxicity.

There are certain limitations to this study. Fusion registrations between MVCT and kVCT images were based on rigid body registration [36]. In the future, nonrigid fusion registration may be required to increase the accuracy of estimated setup error. Deformation is a more complex problem; adequate understanding of global and regional deformation of MVCT images and appropriate software development are required to account for deformation. Soft tissue image resolution with MVCT is poor compared to kVCT images. Enhancing MVCT resolution may help improve the accuracy of this technique and visual verification of anatomical co-registration.

These results emphasize important features of image-guided radiotherapy (IGRT):

- daily patient localization using 3D image guidance is essential to reduce uncertainty in localization,
- setup error evaluation should be performed daily for all treatment regions, preferably for all treatment fractions, and
- systematic monitoring of setup error should be integrated into quality assurance practices for targeted therapies.

If such practices are implemented, scientific decisions can be made as to whether consecutive follow-up imaging is required. Without proper and systematic assessment of limits of IGRT modalities, the precision of targeted therapy is questionable. The use of larger daily or total doses is also becoming more common and demands exquisite attention to detail and precision in the planning and delivery of radiation.

Conclusion

The present study emphasizes the importance of daily three dimensional imaging in all conformal and IGRT radiation therapy. Daily MVCT imaging in Tomotherapy and by extension in all IMRT IGRT treatments is essential to compare and assess the accuracy of treatment delivery to different anatomical locations. This study also emphasizes the importance of monitoring setup error for all treatment fractions.

Corresponding address

S.K. Hui
Department of Therapeutic Radiology – Radiation Oncology, University of Minnesota Medical School
420 Delaware Street SE, Mayo Mail Code 494, 55455 Minneapolis
MN
USA
huixx019@umn.edu

Acknowledgment. We would like to thank Drs. Parham Alaei, Bruce Gerbi, Patrick Higgins, Yoichi Watanabe, Chung Lee, and Chinsoo Cho for their helpful

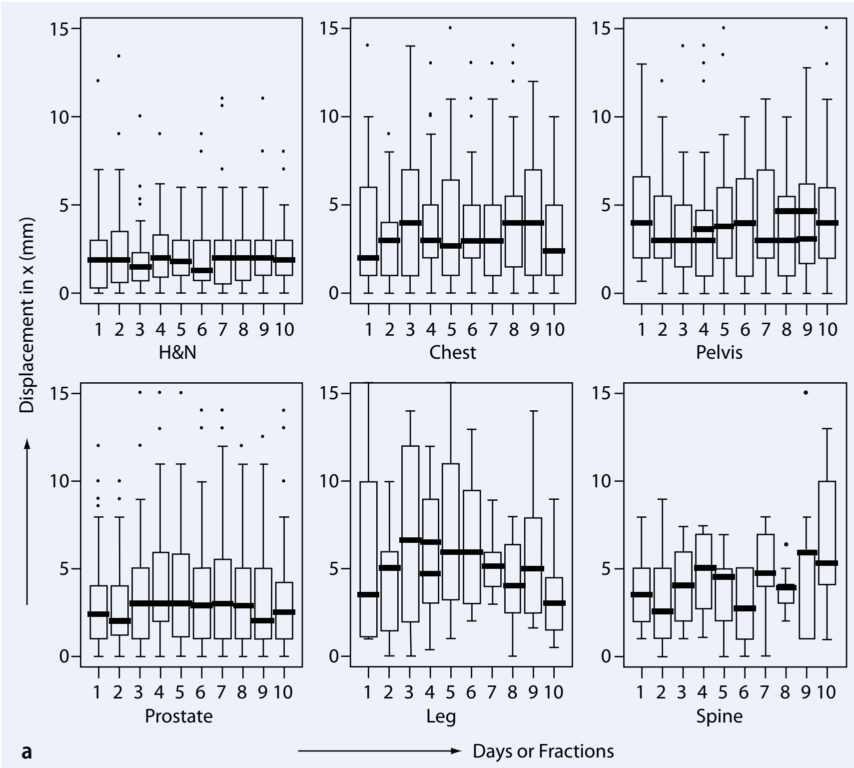

Fig. 2 ▲ Summary of setup error variation with time in the **a** x direction, **b** y direction, and **c** z direction for different radiation treatments. *H&N* head and neck

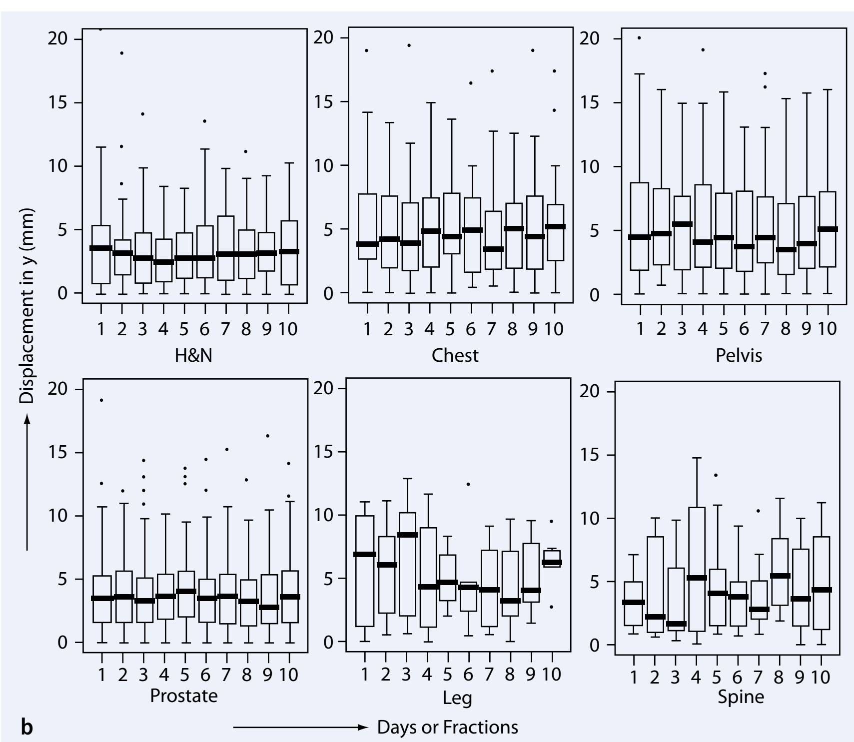

Fig. 2 ▲ continued

discussions. This work was supported by the National Institute of Health grants (1R01CA154491–01). Susanta K Hui is a scholar of the BIRCWH (Building Interdisciplinary Careers in Women's Health) program funded by the National Institute of Child Health and Human Development (NICHD) (1K12-HD055887-01). This work was also supported by PHS Cancer Center Support Grant P30 CA77398.

Conflict of interest. The corresponding author states that there are no conflicts of interest.

References

1. Neal A, Oldham M, Dearnaley D (1995) Comparison of treatment techniques for conformal radiotherapy of the prostate using dose-volume histograms and normal tissue complication probabilities. Radiother Oncol 37(1):29–34
2. Webb S (1991) Optimization by simulated annealing of three-dimensional conformal treatment planning for radiation fields defined by a multileaf collimator. Phys Med Biol 36(9):1201–1226
3. Lauve A, Morris M, Schmidt-Ullrich R et al (2004) Simultaneous integrated boost intensity-modulated radiotherapy for locally advanced head-and-neck squamous cell carcinomas: II—clinical results. Int J Radiat Oncol Biol Phys 60(2):374–387
4. Wolden S, Chen W, Pfister D et al (2006) Intensity-modulated radiation therapy (IMRT) for nasopharynx cancer: update of the Memorial Sloan-Kettering experience. Int J Radiat Oncol Biol Phys 64(1):57–62
5. Bohrer M, Schröder P, Welzel G et al (2008) Reduced rectal toxicity with ultrasound-based image guided radiotherapy using BAT™(B-mode acquisition and targeting system) for prostate cancer. Strahlenther Onkol 184(12):674–678
6. Guckenberger M, Ok S, Polat B et al (2010) Toxicity after intensity-modulated, image-guided radiotherapy for prostate cancer. Strahlenther Onkol 186(10):535–543
7. Stock M, Dörr W, Stromberger C et al (2010) Investigations on parotid gland recovery after IMRT in head and neck tumor patients. Strahlenther Onkol 186(12):665–671
8. Kitamura K, Court LE, Dong L (2003) Comparison of imaging modalities for image-guided radiation therapy (IGRT). Nippon Igaku Hoshasen Gakkai Zasshi 63(9):574–578
9. Lefkopoulos D, Ferreira I, Isambert A et al (2007) Present and future of the image guided radiotherapy (IGRT) and its applications in lung cancer treatment. Cancer Radiother 11(1–2):23–31
10. Ling CC, Yorke E, Fuks Z (2006) From IMRT to IGRT: frontierland or neverland? Radiother Oncol 78(2):119–122
11. Meeks SL, Harmon JF, Jr, Langen KM et al (2005) Performance characterization of megavoltage computed tomography imaging on a helical tomotherapy unit. Med Phys 32(8):2673–2681
12. Rimmer YL, Benson RJ, Routsis DS et al (2007) Image guided radiotherapy (IGRT) in prostate carcinoma: visualisation of implanted fiducial markers. Clin Oncol (R Coll Radiol) 19(3):44
13. Sorensen S, Mitschke M, Solberg T (2007) Cone-beam CT using a mobile C-arm: a registration solution for IGRT with an optical tracking system. Phys Med Biol 52(12):3389–3404
14. Tomsej M (2006) The TomoTherapy Hi.Art System for sophisticated IMRT and IGRT with helical delivery: Recent developments and clinical applications. Cancer Radiother 10(5):288–295
15. Nairz O, Merz F, Deutschmann H et al (2008) A strategy for the use of image-guided radiotherapy (IGRT) on linear accelerators and its impact on treatment margins for prostate cancer patients. Strahlenther Onkol 184(12):663–667
16. Richter A, Sweeney R, Baier K et al (2009) Effect of breathing motion in radiotherapy of breast cancer. Strahlenther Onkol 185(7):425–430

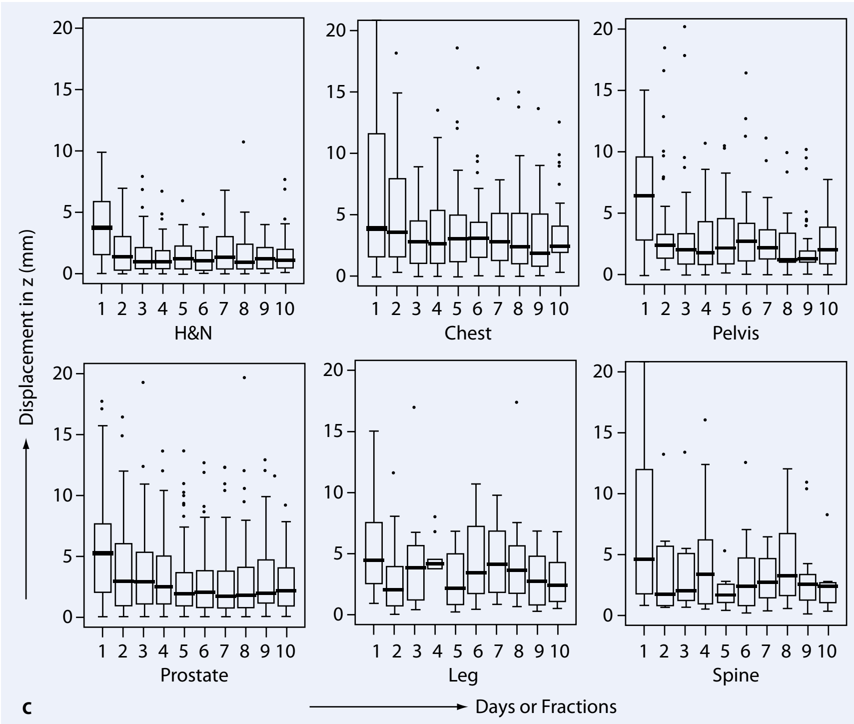

Fig. 2 ▲ continued

17. Tsai CL, Wu JK, Wang CW et al (2009) Using cone-beam computed tomography to evaluate the impact of bladder filling status on target position in prostate radiotherapy. Strahlenther Onkol 185(9):588–595
18. Boda-Heggemann J, Lohr F, Wenz F et al (2011) kV Cone-beam CT-based IGRT: a clinical review. Strahlenther Onkol 187(5):284–291
19. Fodor A, Fiorino C, Dell'oca I et al (2011) PET-guided dose escalation tomotherapy in malignant pleural mesothelioma. Strahlenther Onkol 187(11):736–743
20. Hunt M, Kutcher G, Burman C et al (1993) The effect of setup uncertainties on the treatment of nasopharynx cancer. Int J Radiat Oncol Biol Phys 27(2):437
21. Guckenberger M, Meyer J, Wilbert J et al (2007) Precision of image-guided radiotherapy (IGRT) in six degrees of freedom and limitations in clinical practice. Strahlenther Onkol 183(6):307–313
22. Delana A, Menegotti L, Bolner A et al (2009) Impact of residual setup error on parotid gland dose in intensity-modulated radiation herapy with or without planning organ-at-risk margin. Strahlenther Onkol 185(7):453–459
23. Vorwerk H, Liersch T, Rothe H et al (2009) Gold markers for tumor localization and target volume delineation in radiotherapy for rectal cancer. Strahlenther Onkol 185(2):127–133
24. Hui SK, Das RK, Kapatoes J et al (2004) Helical tomotherapy as a means of delivering accelerated partial breast irradiation. Technol Cancer Res Treat 3(6):639–646
25. Jeraj R, Mackie TR, Balog J et al (2004) Radiation characteristics of helical tomotherapy. Med Phys 31(2):396–404
26. Kapatoes JM, Olivera GH, Balog JP et al (2001) On the accuracy and effectiveness of dose reconstruction for tomotherapy. Phys Med Biol 46(4):943–966
27. Mackie TR, Holmes T, Swerdloff S et al (1993) Tomotherapy: a new concept for the delivery of dynamic conformal radiotherapy. Med Phys 20(6):1709–1719
28. Ruchala KJ, Olivera GH, Kapatoes JM et al (2000) Megavoltage CT image reconstruction during tomotherapy treatments. Phys Med Biol 45(12):3545–3562
29. Welsh JS, Lock M, Harari PM et al (2006) Clinical implementation of adaptive helical tomotherapy: a unique approach to image-guided intensity modulated radiotherapy. Technol Cancer Res Treat 5(5):465–479
30. De Ridder M, Tournel K, Van Nieuwenhove Y et al (2008) Phase II study of preoperative helical tomotherapy for rectal cancer. Int J Radiat Oncol Biol Phys 70(3):728–734
31. Geets X, Tomsej M, Lee JA et al (2007) Adaptive biological image-guided IMRT with anatomic and functional imaging in pharyngo-laryngeal tumors: Impact on target volume delineation and dose distribution using helical tomotherapy. Radiother Oncol 85(1):105–115
32. Mackie TR, Balog J, Ruchala K et al (1999) Tomotherapy. Semin Radiat Oncol 9(1):108–117
33. Ramsey CR, Langen KM, Kupelian PA et al (2006) A technique for adaptive image-guided helical tomotherapy for lung cancer. Int J Radiat Oncol Biol Phys 64(4):1237–1244
34. Yan D, Vicini F, Wong J, Martinez A (1997) Adaptive radiation therapy. Phys Med Biol 42(1):123–132
35. Yan D, Ziaja E, Jaffray D et al (1998) The use of adaptive radiation therapy to reduce setup error: a prospective clinical study. Int J Radiat Oncol Biol Phys 41(3):715–720
36. Boswell S, Tome W, Jeraj R et al (2006) Automatic registration of megavoltage to kilovoltage CT images in helical tomotherapy: an evaluation of the setup verification process for the special case of a rigid head phantom. Med Phys 33(11):4395–4404
37. Hui SK, Kapatoes J, Fowler J et al (2005) Feasibility study of helical tomotherapy for total body or total marrow irradiation. Med Phys 32(10):3214–3224
38. Hui SK (2007) Helical tomotherapy targeting total bone marrow—first clinical experience at the University of Minnesota. Acta Oncol 46(2):250–255
39. Tukey J (1977) Box-and-whisker plots. Exploratory Data Analysis 39–43
40. Verbeke G, Molenberghs G (2000) Linear mixed models for longitudinal data. Springer Publisher, New York, Heidelberg
41. Tukey J (1991) The philosophy of multiple comparisons. Statistical Science 6:100–116
42. Hui S, Verneris M, Higgins P et al (2007) Helical tomotherapy targeting total bone marrow. First clinical experience at the University of Minnesota. Acta Oncologica 46(2):250–255
43. Hui S, Verneris M, Froelich J et al (2009) Multimodality image guided total marrow irradiation and verification of the dose delivered to the lung, PTV, and thoracic bone in a patient: a case study. Technol Cancer Res Treat 8(1):23–28
44. Schubert L, Westerly D, Tomé W et al (2009) A comprehensive assessment by tumor site of patient setup using daily MVCT imaging from more than 3,800 helical tomotherapy treatments. Int J Radiat Oncol Biol Phys 73(4):1260–1269
45. Broggi S, Cozzarini C, Fiorino C et al (2009) Modeling set-up error by daily MVCT for prostate adjuvant treatment delivered in 20 fractions: implications for the assessment of the optimal correction strategies. Radiother Oncol 93(2):246–252
46. Bortfeld T, Jokivarsi K, Goitein M et al (2002) Effects of intra-fraction motion on IMRT dose delivery: statistical analysis and simulation. Phys Med Biol 47(13):2203–2220